Supporting Information

Rheology of Membrane-Attached Minimal Actin Cortices

Helen Nöding[†#], Markus Schön[‡#], Corinna Reinermann[‡], Nils Dörrer[†], Aileen Kürschner[‡], Burkhard Geil[†], Ingo Mey[‡], Claus Heussinger[§], Andreas Janshoff[†*] and Claudia Steinem[‡*]

[†]Georg August Universität Göttingen, Institut für Physikalische Chemie, Tammannstr. 6, 37077 Göttingen, Germany

[‡]Georg August Universität Göttingen, Institut für Organische und Biomolekulare Chemie, Tammannstr. 2, 37077 Göttingen, Germany

[§]Georg August Universität Göttingen, Institut für Theoretische Physik, Friedrich-Hund-Platz 1, 37077 Göttingen, Germany

#both authors contributed equally to this work.

*corresponding authors A. J. and C. S.:

E-mail: ajansho@gwdg.de, csteine@gwdg.de

Phone: +49 551 39 10633

Fax: +49 551 39 14411

CONTENTS

1. Image processing and analysis ('artificial retina')

Most fluorescence microscopy images of actin networks suffer from low contrast, low signal to noise ratios, and large intensity fluctuations along the actin filaments. While the human eye is still able to detect the fibrous morphology, it turns out that a too simplistic image analysis (e.g., a contrast enhancement followed by intensity thresholding and skeletonization) entirely fails to reproduce these structures. We introduce a technique for image preprocessing that emphasizes the filament structure in such raw images and eliminates noisy intensity fluctuations in background regions. In principal this method assumes (the a-priory knowledge) that the intensity of pixels originates from rod-like, filamentous light sources only and uses a series of 'detectors' sensitive to linear extended intensity profiles. Being highly sensitive to a special kind of motives and nearly blind to objects of different shapes we want to call this technique an 'artificial retina'. The concept of this artificial retina is shown in Figure S1.

In a first step the raw image is reduced into a two-dimensional intensity image and its illumination is equilibrated and stretched into the full intensity range via *Contrast Limited Adaptive Histogram Equalization* (CLAHE). The outcome of this procedure is subjected to a multidimensional convolution with a filter bank that consists of N_f filamentous motives. The convolution transforms the image into a three-dimensional object with N_f layers corresponding to the individual filter responses. Every pixel is now characterized by an N_f-dimensional *feature vector* which holds the information about the filamentous character of the local environment of the pixel. Analyzing the 2D-array of feature vectors gives various insights into the actin network structure underlying the fluorescence image. We obtain a probability that distinguishes filament-pixels from background-pixels and we can visualize the local orientation and local thickness of the network fibers.

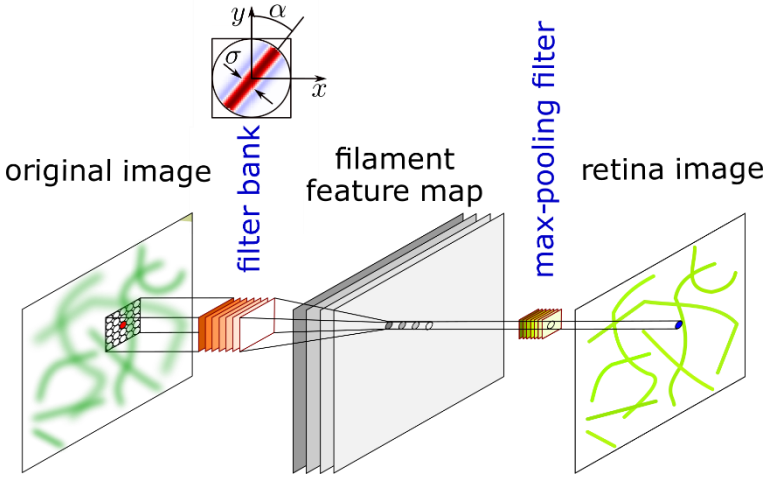

Figure S1. Concept of an 'artificial retina' used as an image preprocessing step in the filament analysis. The inlet shows the parameters of a single filter bank motif.

1.1 A filter bank sensitive to rod-like local structures

The filter bank is constructed by small motives (typical sizes are 21x21 pixels up to 81x81 pixels applied to images of 1000x1000 pixels) containing a centered, rod-like intensity profile modeled by a Mexican-Hat function

$$I(x,y) = \frac{1.0}{\pi \cdot \sigma^2} \cdot \left(1.0 - 0.5 \cdot \frac{x^2}{\sigma^2}\right) \cdot \exp\left(\frac{-0.5 \cdot x^2}{\sigma^2}\right), \quad \text{(S1)}$$

where σ controls the thickness of the rods. The motives are of squared shape with borderlength being an odd number of pixels to ensure that they have a well defined centered pixel. The motiv - here the rod is still aligned parallel to the *y*-axis - is then rotated between 0° and 170° typically in steps of 10° to produce 18 filters of different orientations. The filament thickness sigma is varied between the thinnest and the thickest structures that we want to detect. Typically, a filter bank contains filters with 5 to 10 different sigma values. Thus, a filter bank finally contains in the order of $N_\mathrm{f} = 100$ different motives. It turns out that these filters, even with squared shape, are prone to anisotropic artefacts: rods in 45° orientation are longer than rods of other orientations, leading to diagonal, stripe-like intensity artefacts in the filter response images. Therefore, we mask all motives with a circle exactly fitting into the square and setting the intensity outside of the circle to zero. In a final refinement we renormalize all motives to an integral intensity of zero.

1.2 Final reduction of the feature vectors

Convolution of an image with the filter bank results in pixel-wise N_f-dimensional feature vectors that encode the information of the local network structure. There are several ways to visualize this information.

(1) ***The fiber- or background-character of a pixel*** is obtained by interpreting the value of the largest feature vector component as an intensity. This way one obtains a picture that strongly emphasizes the filaments and smoothens out the noise contained in the raw image. These images are well suited to analyze the filament properties via 'conventional' image analysis, employing intensity thresholding followed by skeletonization.

(2) ***The local orientation of fibrous structures*** is best visualized when all feature vector components that belong to the same alpha-value in the filter bank are added and the maximum of this reduced feature vector is used as a color scheme. Such images reproduce the network structure with colors indicating the local alpha-value.

(3) ***The local filament thickness*** is analyzed in a similar fashion, but now projecting the feature vectors onto a subspace of constant sigma values and using a successive maximum filter to obtain the color scheme.

2. Anisotropy of membrane bound actin networks

The nematic order parameter *q* of the membrane attached F-actin networks was calculated for each skeletonized image according to:[1]

$$q = 2 \cdot \left(\langle \cos^2(\theta_{ij}) \rangle - \frac{1}{2}\right), \quad \text{(S2)}$$

where θ_{ij} is the angle between two filaments i and j.

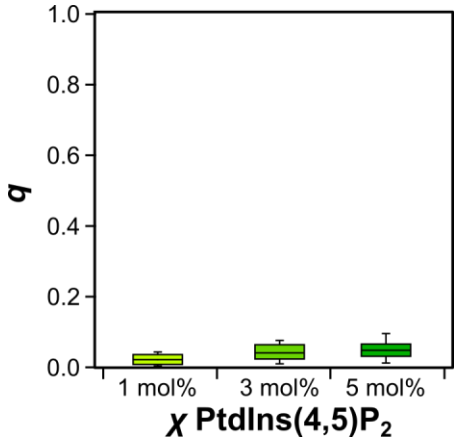

Figure S2. Nematic order parameter *q* of membrane attached F-actin networks. The nematic order parameter was calculated according to eq. (S2) and plotted as a function of the PtdIns(4,5)P_2 concentration in the lipid bilayer.

The order parameter is scaled between 0 and 1, with high values for highly ordered network structures where the filaments are strongly aligned (parallel) and lower values for randomly oriented, unordered filaments. For all networks attached to a lipid bilayer a disordered orientation of the filaments was observed (Figure S2).

3. Mesh size analysis of the membrane-attached actin network

Confocal fluorescence micrographs MACs were subjected to the 'artificial retina' analysis to generate network skeletons. With the skeletonized networks, an Euclidian distance map and therefore the local maxima inside the mesh were obtained.[2] These local maxima serve as center points for circles. In case of overlapping circles inside a mesh, the size of the circles was compared and only the largest one was taken (Figure S3).

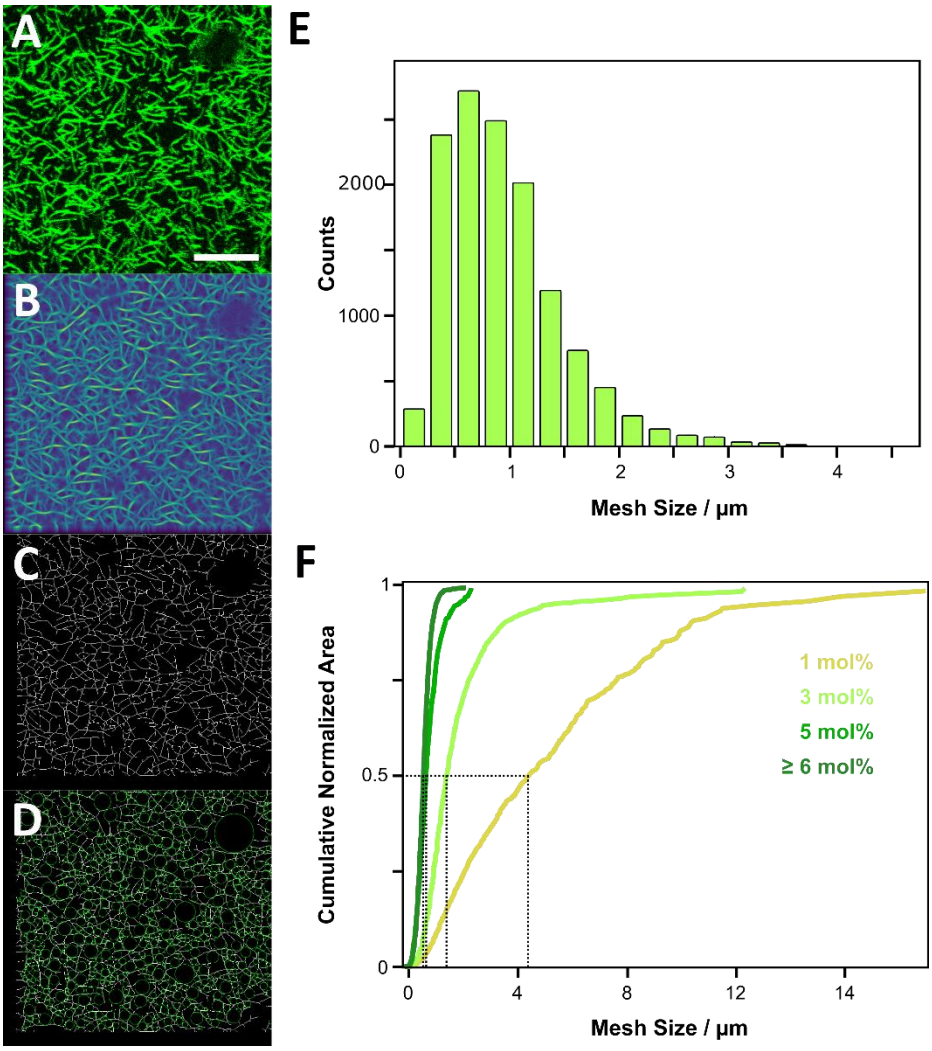

Figure S3. (**A**) Fluorescence micrograph of an F-actin network attached to a lipid bilayer containing 3 mol% PtdIns(4,5)P_2 labeled with AlexaFluor488-phalloidin stained F-actin reveals the network architecture. Scale bar: 5 µm (bottom right). (**B**) 'Artificial retina' analysis of the image shown in (**A**) and (C) skeletonization of the F-actin network based on (D). (**D**) With an Euclidian distance map (EDM) the mesh size was obtained by the largest circle fitting into the mesh. (**E**) Histogram analysis of the mesh size diameter (N = 13085, with N the number of circles). Mesh sizes were determined from 27 fluorescence images taken from 6 preparations. An average mesh size of 0.8 ± 0.5 µm (mean ± SD) was obtained. (**F**) Cumulative normalized area analysis of mesh sizes. Mesh sizes were weighted by the circle area to show the dependency of PtdIns(4,5)P_2 content. Median values are 4.5 µm (1mol%), 1.6 µm (3 mol%), 0.8 µm (5 mol%) and 0.7 µm (≥ 6 mol%).

4. Filament analysis of the actin network

The persistence and the contour length are important characteristic parameters determining the mechanics of actin polymer networks. Actin as a semi-flexible biopolymer has a persistence length[3] l_p = 17 µm in the same range as its contour length L., As the contour length and also the percentage of spontaneous bundling can vary depending on the polymerization conditions, we investigated the diameters of the actin filaments by means of atomic force microscopy.

Sample preparation. Clean and flat glass surfaces (35 mm, No. 1.5, MatTek, Ashland, USA) were incubated overnight with poly-D-lysin (0.1 mg/mL; Sigma-Aldrich, St. Louis, MO). After rinsing the glass surface with actin buffer (50 mM KCl, 20 mM Tris, 2 mM $MgCl_2$, 0.1 mM NaN_3, pH 7.4) 10 µL of pre-polymerized actin filaments (8 µM) were incubated on the sample for 3.5 h (V = 1 mL) and rinsed afterwards.

Atomic force microscopy (AFM) measurements. Images in quantitative imaging mode (≈ 100 nm/pixel) were recorded using a JPK NanoWizard4 atomic force microscope (JPK Instruments, Berlin, Germany). Cantilevers with a sharp tip (r_{nom} = 2 nm) and high sensitivity (MSNL-10, k_{nom} = 100 pN/nm; Bruker AFM Probes, Camarillo, USA) were used for the measurements.

Fiber diameter analysis. AFM images were analyzed to determine the diameters of the pre-polymerized filaments. From line scans it becomes obvious that the height corresponding to filaments (Figure S4A1&2, green) and small bundles are found (Figure S4A1&2, red). For histogram analysis of the diameter distribution, an image was divided in 7×7 quadrants and each filament diameter was counted once per quadrant ((Figure S4B1). The resulting histogram (Figure S4B) reveals primarily single filaments with an average diameter of 9 nm (64 %), which is in accordance with known values form literature.[4,5] Moreover, small bundles with two times the diameter of single filaments (average diameter of 16 nm, 27 %) were found. Only 9 % thicker bundles are observed. From these results we can safely assume the persistence length to be 17 µm and a bending modulus of $\kappa = l_p \cdot k_B T \approx 7 \cdot 10^{-26}$ Nm^2. The contour length L is estimated from a frequency dependent viscoelastic spectrum of purely entangled actin networks (Figure S4A) according to the polymer theory by Morse to be around $L \approx 14$ µm for our polymerization conditions.[6]

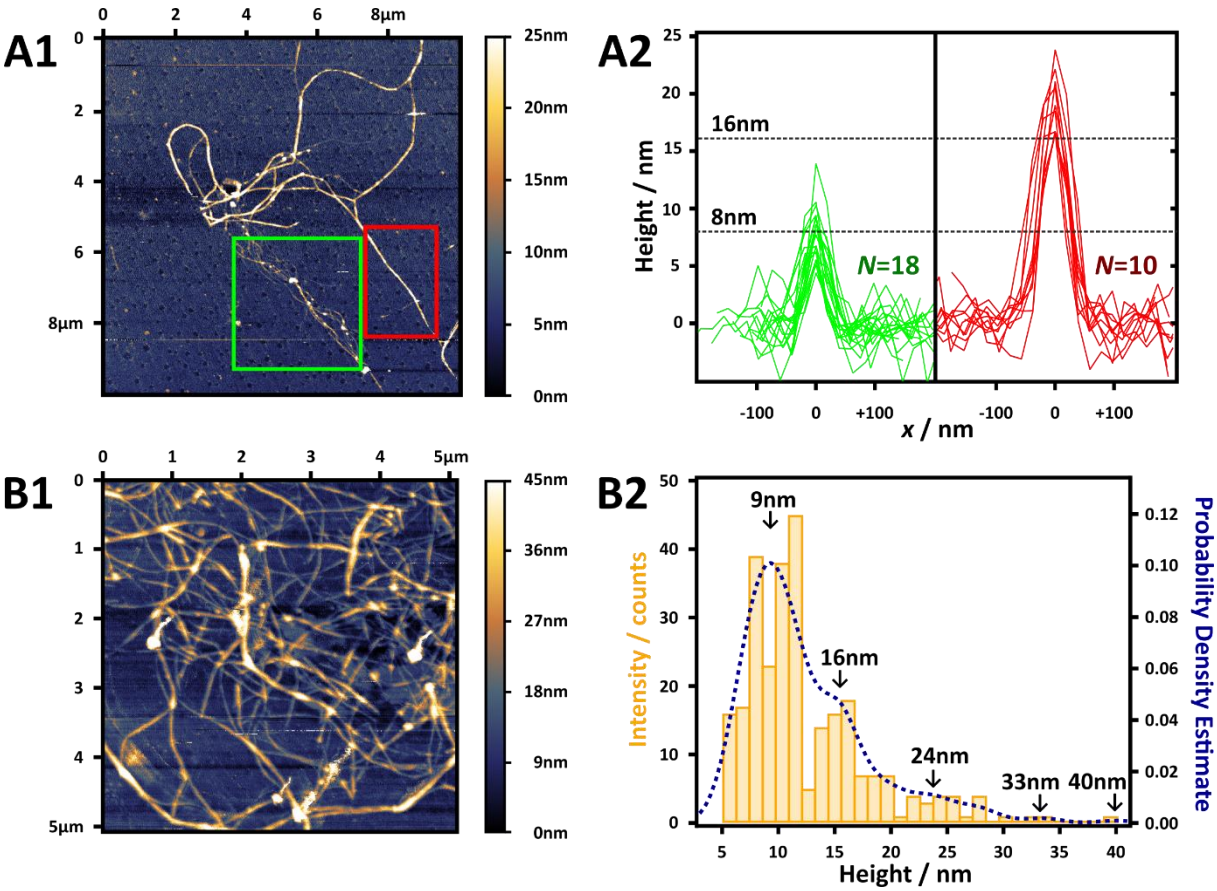

Figure S4. Analysis of the actin filament diameter by atomic force microscopy. (**A1**/**B1**) Atomic force microscopy images of pre-polymerized F-actin attached to a surface via poly-D-lysine. (**A2**) Line scans along the filaments enframed in **A1**. From the line scans an average filament diameter of d = (7.9 ± 2.4) nm (green box, N = 18) and d = (19.1 ± 2.6) nm (red box, N = 10) was determined. (**B2**) Histogram analysis of the diameter distribution of actin fibers (N = 277) indicating primarily single filaments with an average diameter of 9 nm and small bundles with an average diameter of 16 nm.

5. Incorporation of tracer particles in the F-actin filament network

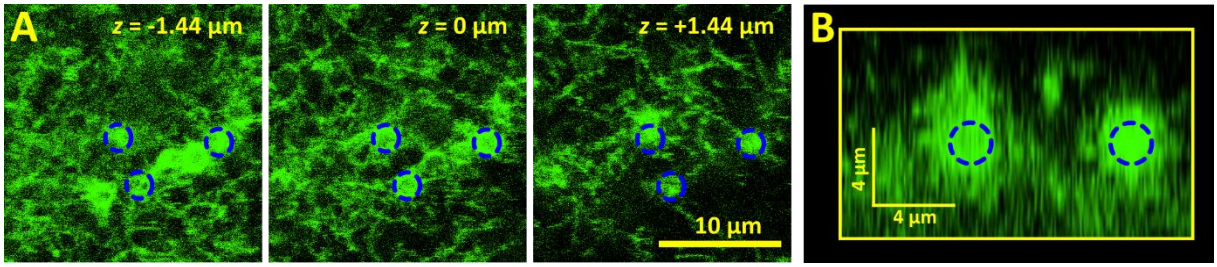

Figure S5. Incorporation of tracer particles in the F-actin network. Confocal fluorescence images of actin networks fluorescently labeled with AlexaFluor488-phalloidin (Life Technologies, Carlsbad, USA) attached to a lipid membrane via ezrin containing 3 mol% PtdIns(4,5)P_2. To show that the F-actin network organizes around the silica surface, non-fluorescent silica particles (Bangs Laboratories, Indiana, USA) with a size of d = 2 µm were used. (**A**) x-y-planes at three different z-positions, at the plane of the tracer particles (z = 0 µm), two planes below (z = -1.44 µm) and two planes above (z = + 1.44 µm). Estimated bead positions are marked with blue dotted lines. (**B**) x-z-plane.

6. The impact of filament length on the frequency dependent viscoelastic properties of F-actin networks

The average contour length L of a filament can be derived from microrheological data by applying a relationship derived from a reptation model by Morse:[5]

$$\tau_{\mathrm{rep}} = \frac{L^3 \cdot 2\eta}{\pi \cdot k_{\mathrm{B}} T \cdot ln(\xi/d)}, \qquad \text{(S3)}$$

assuming that the solvent viscosity $\eta = 0.891\ \mathrm{mPa \cdot s}$, the mesh size $\xi = 900\ \mathrm{nm}$ and the diameter $d = 8\ \mathrm{nm}$ of the actin filaments do not change drastically between the experiments in 3D actin samples the contour length of the filaments can be obtained from the reptation time τ_{rep} (marked in Figure S6 as reptation frequency $f_{\mathrm{rep}} = {\tau_{\mathrm{rep}}}^{-1}$). For un-shortened F-actin filaments in the 3D actin sample with a concentration of 8-23 µM a contour length of $L \approx 16.3\ \mu\mathrm{m}$ was found. This corresponds well with previously observed contour lengths in *in vitro* polymerized F-actin filaments (around 10-20 µm according to Käs *et al*.[7]). In living cells, F-actin filaments are substantially shorter (< 2 µm according to Fritzsche *et al*.[8]). The most important difference between these simple actin model systems and the apical cortex of living cells is of cause the absence of regulatory proteins. Cross-linking proteins introduce additional intersections between filaments. Capping and branching actin binding proteins shorten the average length of F-actin filaments.

As a verification that filament reptation dynamics are observed in the low frequency regime of the frequency dependent viscoelastic properties in 3D entangled F-actin solutions, F-actin filaments were shortened by polymerizing actin in presence of gelsolin (F-actin:gelsolin, 750:1 and 2500:1), a known actin capping and severing protein.[9] As the low frequency cross-over of the storage and loss modulus is dependent on the contour length *L* of the filament (see above $f_{\mathrm{rep}} \propto L^{-3}$) an increase in the cross-over frequency for shorter filaments is expected, which is found in the experiments (Figure S6). A clear shift of the low frequency peak of the loss modulus towards higher frequencies is observed. From the reptation frequency the contour length of the filaments in each sample was determined (Table S1).

Table S1. Calculated contour length L in samples with different gelsolin ratios. f_{rep} is the reptation frequency (local maximum in the low frequency regime of the loss modulus, marked in Figure S6) and c_{a} is the G-actin concentration used.

Sample	N	f_{rep} / $\mathrm{s^{-1}}$	L / µm
c_{a} = 8-23 µM	5	0.008	16.3
c_{a} = 23 µM; actin:gelsolin 2500:1	5	0.040	9.5
c_{a} = 26 µM; actin:gelsolin 750:1	5	0.128	6.5

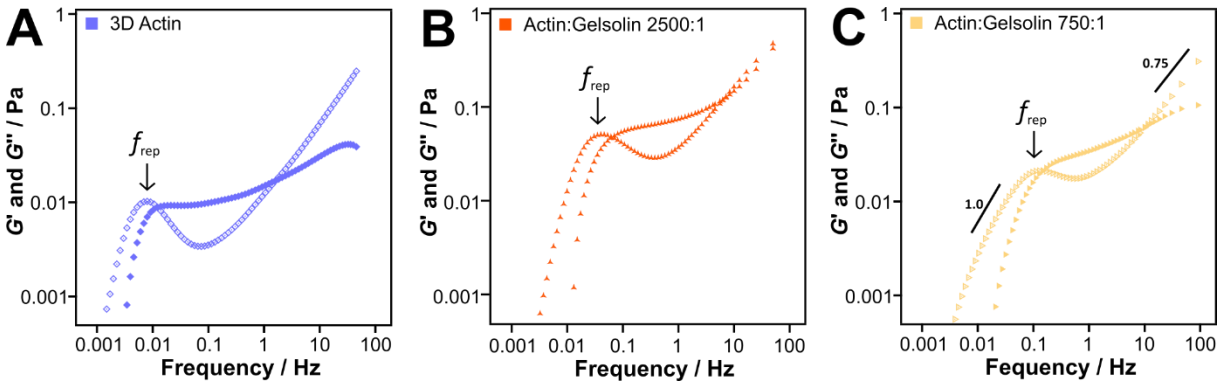

Figure S6. Frequency dependent viscoelastic properties of 3D F-actin networks dependent on the mean filament contour length. Shown are the storage modulus G' (filled symbols), the loss modulus G'' (open symbols) (**A**) Entangled F-actin network (c_a = 8-23 µM, N = 5). (**B**) Entangled F-actin network consisting of actin filaments treated with gelsolin (c_a = 23 µM; actin:gelsolin, 2500:1, N = 5). (**C**) Entangled F-actin network consisting of actin filaments treated with gelsolin (c_a = 26 µM; actin:gelsolin, 750:1, N = 5). Scaling behaviors of 1 in the low frequency regime and 0.75 in the high frequency regime (black solid lines) are plotted in (**C**). N is the number of averaged bead trajectories.

Table S2. Parameters used to model the frequency dependent viscoelastic properties. Eqs. (7) and (8) (1 dispersion) or eqs. (10) and (11) (2 dispersions) were fit to the frequency dependent storage and loss moduli presented in Figure 4 in the main text. Parameters: plateau modulus G_0; cross-over frequency to the high-frequency branch ω_0; friction coefficient relating to cross-linker binding/ unbinding η_i with $i = 1$ for the first dynamic process and $i = 2$ for the second dynamic process. $a_0 - a_3$ are scaling parameters.

	Sample	G_0 /Pa	ω_0 / s^{-1}	η_1 /Pa · s	η_2 /Pa · s	a_0	a_1	a_2	a_3
1 dispersion	Actin 8-23 µM; *N* = 5	0.011 ± 0.0003	0.40 ± 0.14	1.53 ± 0.16	*n. a.*	1.70 ± 0.09	0.43 ± 0.12	*n. a.*	*n. a.*
	PtdIns(4,5)P_2 3 mol%; *N* = 6	0.115 ± 0.004	5.07 ± 1.71	11.82 ± 1.30	*n. a.*	1.25 ± 0.13	0.90 ± 0.32	*n. a.*	*n. a.*
	PtdIns(4,5)P_2 5 mol%; *N* = 9	0.221 ± 0.004	8.14 ± 1.59	22.86 ± 1.18	*n. a.*	1.16 ± 0.06	0.90 ± 0.20	*n. a.*	*n. a.*
2 dispersions	PtdIns(4,5)P_2 3 mol%; *N* = 6	0.116 ± 0.007	1.11 ± 0.81	14.03 ± 0.52	3.28 ± 0.83	1.17 ± 0.09	0.16 ± 0.09	0.32 ± 0.11	0.05 ± 0.06
	PtdIns(4,5)P_2 5 mol%; *N* = 9	0.202 ± 0.013	8.65 ± 1.02	26.45 ± 0.90	6.63 ± 1.06	0.95 ± 0.07	0.80 ± 0.11	0.56 ± 0.16	0.10 ± 0.07

REFERENCES

1. Linsmeier, I.; Banerjee, S.; Oakes, P. W.; Jung, W.; Kim, T.; Murrell, M. P. Disordered Actomyosin Networks are Sufficient to Produce Cooperative and Telescopic Contractility. *Nat. Commun.* **2016**, *7,* 12615.
2. Münster, S.; Fabry, B. A Simplified Implementation of the Bubble Analysis of Biopolymer Network Pores. *Biophys. J.* **2013**, *104,* 2774–2775.
3. Yanagida, T.; Nakase, M.; Nishiyama, K.; Oosawa, F. Direct Observation of Motion of Single F-Actin Filaments in Presence of Myosin. *Nature* **1984**, *307,* 58–60.
4. Blanchoin, L.; Boujemaa-Paterski, R.; Sykes, C.; Plastino, J. Actin Dynamics, Architecture, and Mechanics in Cell Motility. *Physiol. Rev.* **2014**, *94,* 235–263.
5. Grazi, E. What is the Diameter of the Actin Filament? *FEBS Lett.* **1997**, *405,* 249–252.
6. Morse, D. C. Viscoelasticity of Concentrated Isotropic Solutions of Semiflexible Polymers. 2. Linear Response. *Macromolecules* **1998**, *31,* 7044–7067.
7. Käs, J.; Strey, H.; Tang, J. X.; Finger, D.; Ezzell, R.; Sackmann, E.; Janmey, P. A. F-Actin, a Model Polymer for Semiflexible Chains in Dilute, Semidilute, and Liquid Crystalline Solutions. *Biophys. J.* **1996**, *70,* 609–625.
8. Fritzsche, M.; Erlenkämper, C.; Moeendarbary, E.; Charras, G.; Kruse, K. Actin Kinetics Shapes Cortical Network Structure and Mechanics. *Sci. Adv.* **2016**, *2,* e1501337.
9. Janmey, P. A.; Hvidt, S.; Peetermans, J.; Lamb, J.; Ferry, J. D.; Stossel, T. P. Viscoelasticity of F-actin and F-actin/gelsolin complexes. *Biochemistry* **1988**, *27,* 8218–8227.